Transport Phenomena in a Catalytic Monolith: Effect of the Superficial Reaction

A. Di Benedetto and F. S. Marra
Istituto di Ricerche sulla Combustione—C.N.R., P. le Tecchio, 80, 80125 Naples, Italy

F. Donsì and G. Russo
Dipartimento di Ingegneria Chimica—Università degli Studi di Napoli Federico II, P. le Tecchio, 80, 80125 Naples, Italy

DOI 10.1002/aic.10680
Published online October 14, 2005 in Wiley InterScience (www.interscience.wiley.com).

The effect of a fast exothermic surface reaction on the fluid flow and on heat transfer between bulk gas phase, and the catalytic wall in a monolithic reactor has been studied by means of a 2-D mathematical model. The radial profiles of temperature, concentration, and velocity in the ignition region show that the perturbation induced by the reaction is qualitatively comparable to the entrance effects. From the standpoint of heat transfer efficiency the channel may be divided into two zones, the first dominated by the entrance effects and the second dominated by the reaction effects. In the first zone the interphase heat transfer resembles the constant wall heat flux (Nu_H), while after ignition resembles the constant wall temperature (Nu_T) only once the perturbation generated by the reaction ignition has extinguished. It is, hence, showed that the Nu number may be calculated as the interpolation between Nu_H, and a modified Nusselt number Nu_{ad}, which is defined as a function of the difference between the adiabatic temperature and gas bulk temperature rather than wall-gas temperature difference. It is anchored to the ignition location, depends on the operating and kinetic parameters and asymptotically tends to Nu_T. © 2005 American Institute of Chemical Engineers *AIChE J,* 52: 911–923, 2006
Keywords: heat transfer, catalytic reaction, Navier-Stokes equations, monolith reactor, CFD simulation

Introduction

The catalytic oxidation of hydrocarbons in monolithic reactors is increasingly studied for applications ranging from volatiles organic compounds abatement to portable production of heat, from gas turbines combustors to the production of intermediate chemicals.[1,2,3] Their widespread use calls for the development of reliable mathematical models, capable of accurately predicting the behavior of the reacting system, not only in terms of global performance, but also in terms of local values of the main variables, such as temperature or concentration, which may influence the design requirements or material choice.

In the recent years models of monolithic reactors have been developed at different levels of complexity. The choice of complexity of the model is a tradeoff between accuracy required and available computational resources. The most computationally expensive and at the same time the most accurate are the three-dimensional (3-D) models in which energy and mass balances are coupled to the Navier-Stokes equations in the actual channel geometry.[4,5]

A first simplification of the mathematical problem can be introduced in the geometry of the channel, with the hypothesis of axial symmetry, but still maintaining the coupling with the Navier-Stokes equations: many models were developed and adapted to different problems involving catalytic monoliths,

Correspondence concerning this article should be addressed to A. Di Benedetto at dibenede@irc.na.cnr.it.

such as catalytic combustion[6,7] and catalytic partial oxidation.[8] At a lower complexity level are placed 2-D models where Navier-Stokes equations are not solved, and a parabolic or a flat profile of gas velocity is assumed, saving a considerable amount of computing time.[9,10,11]

Nevertheless, at the presently available computer power, the solution of 2- and 3-D models, even under simplifying assumptions, is excessively time-consuming for applications such as real time simulations or kinetic parameters estimation,[12] whereas 1-D models are more desirable. Remarkably, in the presence of a fast exothermic surface reaction the accuracy and reliability of 1-D models lay in the correct evaluation of mass and thermal fluxes between bulk gas phase and surface, via local mass and heat-transfer coefficients, as a mass transfer-limited regime is readily established in the catalytic channel.[13]

In addition, numerical simulations with 2- and 3-D models of the reactive monoliths, from the pioneering investigations performed in the seventies to more recent works,[10,11,13,14,15,16,17] highlighted that in the light-off region mass and heat transfer are greatly enhanced in a not easily predictable way due to the perturbation associated to the fast heat production at the wall. In particular, it was shown by means of numerical simulations based on 2-D models, in which the gas velocity profile is assumed developed, that prior to light-off the wall heat flux can be considered constant due to the low rate of the surface reaction, and after the light-off the wall temperature can be considered constant and equal to the adiabatic temperature.[9,10,11,15] Hence, the Nusselt number resembles the local *Nu* number for heat exchange in ducts (Graetz problem) for the boundary condition of constant wall heat flux (Nu_H) upstream of the light-off and of constant wall temperature (Nu_T) downstream. In the transition from Nu_H to Nu_T the local *Nu* number goes through a maximum in correspondence of the light-off location, which cannot be described by the heat exchanger correlations. The transition between Nu_H and Nu_T in the reactive case was described via their interpolation with the local transverse Damköhler number (Da_t) by Groppi and co-workers.[10,11] Nevertheless, the same authors recognize that in the case of adiabatic conditions more parameters come into play (such as the activation energy and the adiabatic temperature rise), and the axial profiles of *Nu* exhibit a more or less marked spike in correspondence of the catalytic light-off, originated from the sudden change in the boundary conditions which is not reproduced by means of this correlation.[10] Additionally, heat-transfer coefficients were shown to be dependent not only on reaction kinetics, but also on gas inlet temperature, composition, and gas velocity.[13]

Recently, Gupta and Balakotaiah, by solving a 2-D model in which a developed flow field is assumed, confirmed that local heat-transfer coefficients are neither continuous nor unique functions of the axial position along the channel, but depend on reaction parameters, and jump from one asymptote to another at ignition/extinction point.[9] However, they claimed that the local maximum appearing in *Nu* plots at the ignition point is due to numerical inaccuracies associated with the Gibbs phenomenon, arising in the Fourier series representation of a discontinuous function. Hence, the true *Nu* numbers decrease monotonically with a discontinuous jump from Nu_H curve to a lower asymptotic curve (Nu_T).[9]

Our previous article on the subject was devoted to the critical assessment of the enhancement of heat and mass transfer in concurrence with reaction ignition, separately from the entrance effect, by taking into account the coupling between energy, mass, and momentum balance equations. The model of a single channel of a monolithic combustor consisted of two zones: the first one is characterized by noncatalytic walls, and is long enough for assuring the development of fluid temperature, concentration, and velocity profiles, while in the second zone the catalytic reaction takes place. By means of the study of the effect of the superficial reaction on the radial profiles of concentration, temperature, and velocity, separately from the entrance effects, it was shown that a significant enhancement of *Nu* is induced by the perturbation due to the surface reaction not only on temperature and concentration but also on flow field.[6] It was also shown that in the presence of a superficial reaction *Nu* number depends on the adiabatic temperature rise of the mixture, and on the radial component of velocity.

Table 1. Conditions of the Numerical Simulation of the Base Case

Parameter	Value
T_{in} (K)	600
u_{in} (m/s)	36
$Y_{C3H8,in}$	0.015
p (Pa)	105000
λ_w	0

In this article the perturbation induced by the catalytic combustion of propane is studied in the presence of the entrance effects, with the final scope of giving insights on the heat transfer efficiency between wall and bulk gas phase under the simultaneous influence of entrance effects and superficial reaction. To this end, the model of the monolithic channel consists of a single zone, entirely catalytic: the development of the heat, mass, and velocity boundary layers from the uniform inlet conditions is reciprocally influenced by the superficial reaction.

Model Development

A 2-D model has been adopted to simulate the behavior of a circular adiabatic monolith reaction (length $L = 0.12$ m; internal radius $R = 0.00045$ m and external channel radius $R_w = 0.0005$) m in which a superficial reaction occurs. Internal diffusion resistances are neglected and, thus, the reaction occurs at the channel surface. In order to focus the study on the effect of the superficial reaction on heat and mass fluxes, homogeneous reactions have been neglected. Even if this assumption could not be always valid, it covers a large range of practical application. As base case we considered the catalytic combustion of an air-propane mixture entering the channel at typical conditions reported in Table 1. It could be expected that near the wall, the catalyzed reaction can easily ignite the propane-air mixture since the gas temperature becomes higher than the homogeneous propane combustion ignition temperature. Nevertheless, preliminary simulations run with CRESLAF package of CHEMKIN,[18] (with respect to the present model, with the simplification of the boundary layer assumption), including a detailed homogeneous chemistry (GRI-Mech[19]), showed that the channel residence time is too short to allow homogeneous reaction ignition.

In this article numerical simulations of the behavior of the monolith, and the computed heat-transfer efficiency are compared with the solution of heat transfer in the absence of

reaction with fixed heat flux at the wall (Nu_H) or fixed wall temperature (Nu_T).

Governing equations

The mass and energy balance equations have been solved coupled to the Navier-Stokes equations.

The unsteady balance equations have been solved and here reported, nevertheless only steady-state results will be presented in this article. It is worth to note that the solution of the full transient, for the adopted numerical solver, has been proved more efficient than the direct solution of the steady state form of the equations, due to the presence of the strong gradient present at the wall at the steady state, which is allowed to smoothly develop during the transient phase.

The balance equations are written in cylindrical co-ordinates and they read

Continuity equation:

$$\frac{\partial \rho}{\partial t} + \frac{\partial \rho u}{\partial z} + \frac{1}{r}\frac{\partial r \rho v}{\partial r} = 0 \tag{1}$$

Momentum balance equation in the axial co-ordinate

$$\frac{\partial \rho u}{\partial t} + \frac{\partial \rho u u}{\partial z} + \frac{1}{r}\frac{\partial r \rho v u}{\partial r} = -\frac{\partial p}{\partial z} + \frac{1}{r}\frac{\partial r \tau_{zr}}{\partial r} + \frac{\partial \tau_{zz}}{\partial z} \tag{2}$$

Momentum balance equation in the radial co-ordinate:

$$\frac{\partial \rho v}{\partial t} + \frac{\partial \rho u v}{\partial z} + \frac{1}{r}\frac{\partial r \rho v v}{\partial r} = -\frac{\partial p}{\partial r} + \frac{\partial \tau_{zr}}{\partial z} + \frac{1}{r}\frac{\partial r \tau_{rr}}{\partial r} \tag{3}$$

Specie mass balance equation:

$$\frac{\partial \rho y_i}{\partial t} + \frac{\partial \rho u y_i}{\partial z} + \frac{1}{r}\frac{\partial r \rho v y_i}{\partial r} = \frac{\partial}{\partial z}(J_{z,i}) + \frac{1}{r}\frac{\partial}{\partial r}(rJ_{r,i}) \qquad i = 1, \ldots, N_s - 1 \tag{4}$$

Gas energy balance equation:

$$\frac{\partial \rho h}{\partial t} + \frac{\partial \rho u h}{\partial z} + \frac{1}{r}\frac{\partial r \rho v h}{\partial r} = \frac{\partial}{\partial z}\left(\lambda \frac{\partial T}{\partial z}\right) + \frac{1}{r}\frac{\partial}{\partial r}\left(r\lambda \frac{\partial T}{\partial r}\right) + \frac{\partial p}{\partial t} \tag{5}$$

Solid energy balance equation:

$$\frac{\partial \rho_w h_w}{\partial t} = \frac{\partial}{\partial z}\left(\lambda_w \frac{\partial T_w}{\partial z}\right) + \frac{1}{r}\frac{\partial}{\partial r}\left(r\lambda_w \frac{\partial T_w}{\partial r}\right) \tag{6}$$

where $h = c_p(T)T + \sum_{i=1}^{N_S} y_i H_i^0 + p/\rho + (u^2 + v^2)/2$, and N_s is the number of species that form the gas mixture. Diffusive mass fluxes $J_{r,i}$ and $J_{z,i}$ are computed as:

$$J_{x,i} = \mu Sc \frac{\partial y_i}{\partial x} \quad x = r, z \tag{7}$$

where Sc is the Schmidt number ($Sc = 0.7$), and μ is the dynamic viscosity. Ideal gas law completes the model. The boundary conditions are the following:

$$@\ z = 0 \text{ and } 0 < r < R: \quad u = u_{\text{in}},\ v = 0,\ T = T_{\text{in}},\ y_i = y_{i,\text{in}} \tag{8}$$

$$@\ z = L \text{ and } 0 < r < R: \quad \frac{\partial u}{\partial r} = v = \frac{\partial T}{\partial r} = \frac{\partial y_i}{\partial r} = 0 \tag{9}$$

$$@\ 0 < z < L \text{ and } r = 0: \quad \frac{\partial u}{\partial r} = v = \frac{\partial T}{\partial r} = \frac{\partial y_i}{\partial r} = 0 \tag{10}$$

$$@\ 0 < z < L \text{ and } r = R: \quad u = v = 0$$

$$@\ z = 0 \text{ or } z = L \text{ and } R < r < R_w: \quad \frac{\partial T_w}{\partial z} = 0$$

$$@\ 0 < z < L \text{ and } r = R_w: \quad \frac{\partial T}{\partial r} = 0 \tag{11}$$

At the channel surface wall ($@\ 0 < z < L$ and $r = R$) the reaction occurs and the following boundary condition apply:

$$@\ 0 < z < L \text{ and } r = R: \quad \lambda \left.\frac{\partial T}{\partial r}\right|_{-} = \lambda_w \left.\frac{\partial T_w}{\partial r}\right|_{+} + \omega_h,\ J_{r,i}|_{-} = \omega_{y,i}; \tag{12}$$

Reaction occurs at the channel surface. The source terms ω_h and $\omega_{y,i}$ that appear in the gas boundary conditions for energy and species mass balance equations represent the rate of heat generated by the chemical reaction, and the rate of reaction of species i, respectively.

The base case model reaction is the catalytic combustion of propane. The reaction rate is assumed to be a one step irreversible reaction zeroth order with respect to oxygen and first order with respect to propane mass fraction as following

$$\omega_{y,C_3H_8} = k_0 \exp\left(-\frac{\Delta E}{\bar{R}T}\right) y_{C_3H_8} \tag{13}$$

and, therefore

$$\omega_h = \omega_{y,C3H8} \Delta H_{C3H8} \tag{14}$$

being ΔH_{C3H8} the heat of combustion of propane. The values of the adopted kinetic parameters are $k_0 = 10^6$ mol/m^2 s, $\Delta E/\bar{R} = 10869$ K.[1]

A single step reaction is an oversimplification of the mechanism of oxidation of propane on a catalytic surface. Nevertheless, the use of a detailed surface mechanism goes beyond the scope of this work, which is to investigated the effect of the superficial reaction on the interphase heat and mass transfer, under general operating conditions, hence, at varying parameters, ranging from the inlet conditions to the catalyst activity, and to identify the link between ignition and heat and mass

fluxes rather than identifying the exact position of light-off, with reference to a specific catalyst and/or reactive mixture.

Viscosity was calculated by means of multicomponent mixture approach, specific heats of the species are determined from the Janaf tables, thermal conductivity and diffusivity by means of the Pr (Sc) number value fixed at 0.7.

From the computed solution of the numerical model, the radial average variable (ϕ_b), gas temperatures (T_b), and propane mass fractions (y_b) have been calculated according to the following formula

$$\phi_b = \frac{\int_0^R \rho\phi u r dr}{\int_0^R \rho u r dr} \tag{15}$$

Nu and Sh numbers have been calculated at bulk conditions, according to the following formulae

$$Nu = \frac{\lambda(T_w)}{\lambda(T_b)} \frac{2R}{T_w - T_b} \left.\frac{\partial T}{\partial r}\right|_{r=R} \tag{16}$$

$$Sh = \frac{D(T_w)}{D(T_b)} \frac{2R}{y_w - y_b} \left.\frac{\partial y}{\partial r}\right|_{r=R} \tag{17}$$

where T_w and y_w are the gas temperature and propane mass fraction computed at the wall.

Moreover, the friction coefficient C_f defined as the ratio between the wall attrition and the inertia in the bulk gas phase is calculated as follows

$$C_f = \frac{8\tau_w}{\rho_b u_b^2} \tag{18}$$

This fact allows to quantify the momentum transfer from the bulk gas phase to the wall.

Numerical solution

The model Eqs. 1–6 have been discretized by adopting the control volume approach which allows a weak solution.[20] In the present case this approach is necessary as the light-off point may give rise to very steep temperature, concentration, and velocity profiles as a consequence of the jump from the non-ignited to the ignited solution.[9] Indeed, it is known that numerical solutions that exhibit large gradients are usually accompanied by the Gibbs phenomenon leading to spurious and unphysical oscillations. This is particularly severe in the vicinity of shocks but it is possible also when solutions are smooth but have steep gradients. As stated by the Godunov's theorem,[20] reconciling high accuracy and absence of spurious oscillations is a difficult task. To overcome this numerical difficulty in the literature a large variety of numerical schemes was proposed. Linear schemes (whose coefficients are not dependent on solution) of order higher than one are accurate, but not able to ensure that the solution is bounded. Conversely, linear schemes of order one, as the upwind scheme, guarantee that the numerical solution is bounded between the extreme values of the analytical solution by introducing a numerical viscosity, thus smearing the jump over a large extent.

Only nonlinear high-order schemes can ensure both high accuracy and boundedness of the solution if very steep gradients arise in the solution.[20] In this article, we adopted the SMART scheme developed by Gaskell and Lau (1988).[21] This scheme is conservative, bounded and accurate. Indeed, it blends the second-order upwind scheme in the region of smooth variation of the variables, and the first-order upwind in region where steep gradients are present, minimizing the amount of numerical viscosity added at the price of slower convergence and computational complexity. A central scheme has been used for all diffusive terms. Time advance is performed through the explicit first order Euler scheme.

Numerical solutions have been performed by means of the commercial software package CFD-ACE+.[22] The resulting system of nonlinear algebraic equations has been solved following the SIMPLEC method.[23] The remaining conditions of the base case simulation are given in Table 1.

The accuracy of numerical results was tested performing simulations at different grid refinements. The axial mesh size was changed in order to test the accuracy of the numerical scheme of capturing the light-off position. In any cases, the grid was chosen to be finer in the zone of light-off along the axial direction, and in the proximity of the wall along the radial direction. It is worth saying that the grid was adapted to the changes of the kinetic parameters that determine a variation of the location of the light-off point.

The used grid consists on 400 cells along z and 48 cells along r. A complete simulation takes about 24 h of CPU time on a AMD 2100+ PC to reach a converged solution starting from nonignited conditions.

Results

Phenomenology at the ignition point

The numerical solution for the base case described in Table 1 is reported in Figure 1 as a function of the dimensional coordinate z, and of the dimensionless coordinate x^*. The dimensionless co-ordinate x^* was calculated as function of the Re number based on the channel diameter and evaluated at the inlet conditions and Pr number, which is assumed equal to 0.7: $x^* = z/(Re\ Pr\ 2R)$.

Light-off location is highlighted by the strong variation of the axial profiles of temperature and concentration, with the wall temperature rising to the adiabatic value and the wall propane concentration dropping to zero (Figure 1). Indeed, from $x^* = 6.8 \cdot 10^{-4}$ ($z = 2.7 \cdot 10^{-4}$ m), the surface reaction is ignited and the rate of reaction and of heat generation at the wall becomes faster than the rate of heat and mass transfer to the bulk of the gas.

The onset of strong external diffusion resistance determines the establishment of large differences between the wall and the bulk values. For instance, while the wall temperature rapidly rises up to the adiabatic temperature, the bulk of the gas is only gradually heated, determining a difference between the wall, and the bulk temperature up to 550 K, and an analogous trend can be observed for propane mass fraction.

The transverse Damköhler number Da_t (Eq. 19), which corresponds to the ratio between the wall concentration, and the difference between the bulk and the wall concentration plotted in Figure 1, gives an estimation of the regime controlling the superficial reaction.[11,16] Prior to light-off Da_t is much

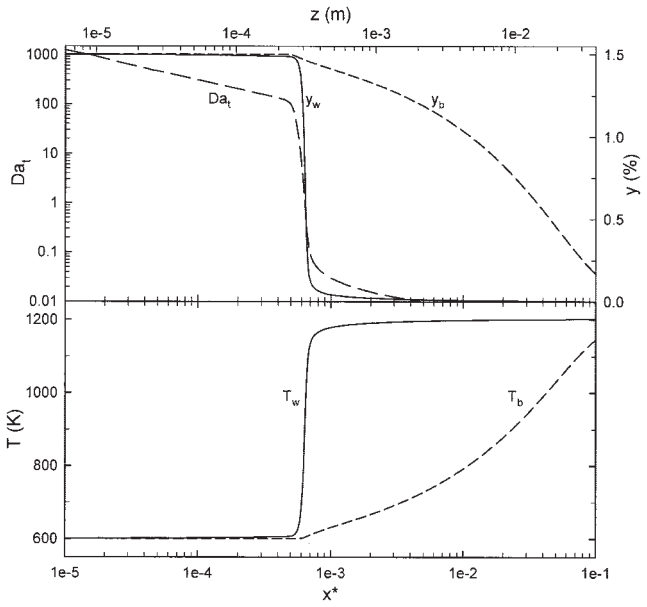

Figure 1. Transverse Damköhler number (Da_t), wall and bulk propane concentration (y_w, y_b), and wall and bulk temperature (T_w, T_b) as a function of the axial actual (z), and dimensionless coordinate (x^*).

higher than 10, as the reaction is controlled by the intrinsic kinetics. After light-off Da_t drops to extremely low values, meaning that the reaction is under interphase mass and heat transfer control. In accordance, the drop of Da_t corresponds to the drop of the propane mass fraction at the wall, and to the rapid rise of wall temperature.

$$Da_t = \frac{L\omega_{C_3H_8}}{u_{\text{in}}C_{C_3H_8}R} \tag{19}$$

In the ignition region the development of new heat and mass boundary layers can be observed, as shown in Figure 2a and b, where the profiles of temperature (a) and propane mass fraction (b), are reported. The formation of new heat and mass boundary layers is usually reckoned as responsible of the increase in mass and heat transfer efficiency.[1,10,11,13,17]

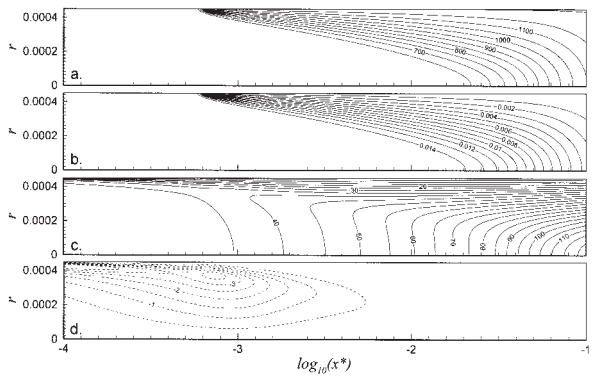

Figure 2. Temperature (a), propane mass fraction (b), axial (c), and radial (d) velocity as function of x^* and r.

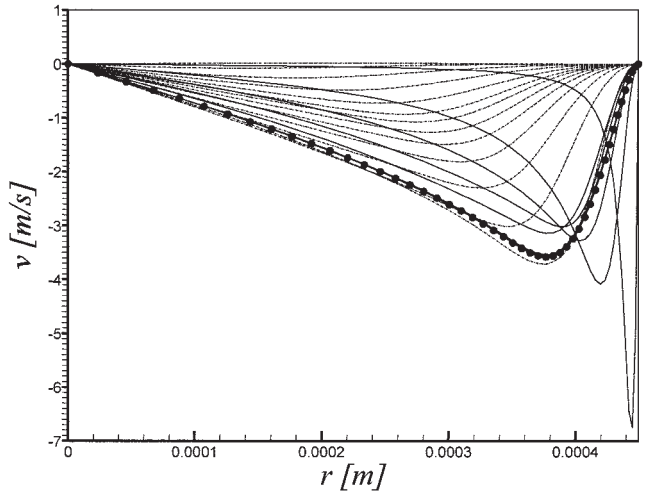

Figure 3. Radial component of velocity (v) vs. the channel radius (r) at different values of the axial position, prior to light-off (—), after light-off (- - -), and at light-off location (●).

The ignition of the reaction takes place in a region where the entrance effects are still strongly present. The hydrodynamic length, which is defined as the duct length required to achieve a maximum duct section velocity of 99% of that for fully developed flow when the entering profile is uniform, indeed corresponds to $x^*_{hy} = 0.08$ ($z = 0.0322$ m),[24,27] and, hence, largely embeds the ignition location. It is ineluctable that the entrance effects play an important role on the light-off location.

Vice versa, the occurrence of the superficial reaction strongly affects also the flow field. In Figure 2c and d the profiles of the axial and radial component of velocity are, respectively, shown. The axial component of velocity u (Figure 2c), which is flat at the inlet, develops towards a parabolic profile, and at the ignition is accelerated by the gas expansion generated by the heat production at the wall. In concurrence with the acceleration of u a strong radial component of velocity v (Figure 2d) arises: after a first perturbation at the inlet due to the entrance effects, where a negative peak in the very proximity of the wall is attained ($r = 4.4 \cdot 10^{-4}$ m), another perturbation in the form of a negative peak can be detected in the light-off region, due to the deviation of the streamlines associated to the gas expansion.

In any case the radial component of velocity is directed from the wall to the center of the channel. In the region where entrance effects are present, the velocity peak is located very close to the wall; conversely, when determined by the ignition, the peak is more shifted towards the centre of the channel, at a radius $r = 3.7 \cdot 10^{-4}$ m. This behavior is related to the fact that the perturbation due to the ignition acts on the velocity profile, already perturbed by the entrance effect, by increasing its value rather than qualitatively changing the fluid flow profiles. The perturbations on both the radial and the axial component of velocity are better shown in Figure 3 and Figure 4, where v and u are, respectively, reported as a function of the channel radius at various axial positions.

Curves corresponding to positions upstream of the light-off

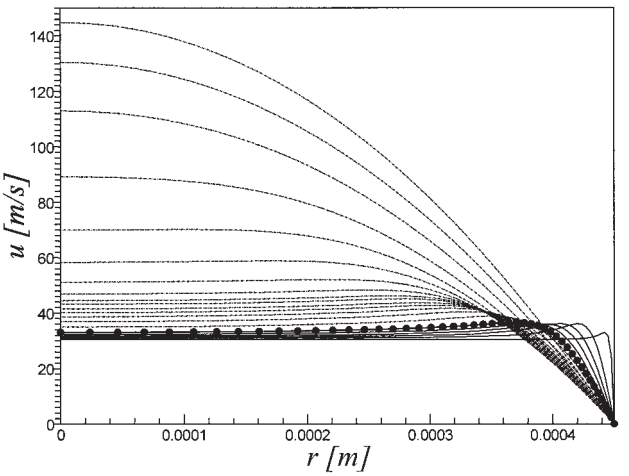

Figure 4. Axial component of velocity (*u*) vs. the channel radius (*r*) at different values of the axial position, prior to light-off (—), after light-off (- - -), and at light-off location (●).

are indicated by the solid lines (—). The thicker profile with symbols (●) identifies the light-off location. Dashed lines (- - -) are adopted to represent the profiles downstream the light-off section. Prior to light-off (—), the arising of the radial component of velocity is due to the entrance effects as the fluid streamlines are shifted towards the centre of the channel. Such perturbation acts very close to the wall, where the flow streams suddenly slow down from the inlet velocity to zero.

In the development of the parabolic profile of velocity, v decreases tending to zero, as indicated by the trend of the solid lines (—). Nevertheless, the occurrence of the ignition, with the consequent gas expansion at the wall, determines a significant increase of v (●), whose profile is not affected in shape but in intensity. Downstream of the ignition the radial velocity again decreases and correspondingly a parabolic profile develops (- - -).

An analogous behavior is exhibited by the axial component of velocity (u), which is accelerated but not deformed in corresponds of light-off.

Numerical results clearly show that the development of the flow field from the flat inlet conditions is significantly affected in the ignition region, and the nature of such perturbation consists in the rapid heating of the gas near the wall, with consequent acceleration of the stream both in axial and radial directions.

Transfer efficiency

The phenomenological analysis of the ignition in a monolith suggests that in the light-off region new radial concentration, temperature, and velocity profiles develop.

In Figure 5 the transfer efficiency of mass, heat, and momentum from the bulk to the wall are reported, respectively, in the form of the Sherwood number (*Sh*, defined in Eq. 17), Nusselt number (*Nu*, defined in Eq. 16), and the friction coefficient C_f (defined in Eq. 18), computed from the numerical solution.

Sh and *Nu* are compared with the *Nu* numbers we calculated for forced convection in ducts in the case of constant wall heat flux (Nu_H), and constant wall temperature (Nu_T) in a previous work.[25] Indeed, our curves of Nu_T and Nu_H are slightly different from those reported in literature,[24] as they are here calculated from the solution of the full Navier-Stokes equations without any simplification.

Nu and *Sh,* for the case considered herein ($Pr = Sc$), exhibit the same trend and, hence, in the following only *Nu* will be discussed. In the ignition region a small difference can be observed between *Nu* and *Sh,* with the *Nu* spike slightly higher than the *Sh* spike. This difference was already discussed and attributed to the convective contribution to interphase transfer associated to the rise of the radial component of velocity, which acts in opposite direction for mass and heat transport.[26]

Upstream of the ignition *Nu* resembles Nu_H, while downstream tends asymptotically to Nu_T. Indeed, the heat exchange prior to light-off can be assimilated to a constant wall heat flux problem due to the slow rate of reaction, while downstream of ignition, when the wall temperature has steadily reached the adiabatic temperature ($T_w = T_{ad}$) the heat exchange can be assimilated to a constant wall temperature problem. This behavior is confirmed by the results reported in literature.[9,10,11,13,14,15,16,17]

In the light-off region the Nusselt number does not match the

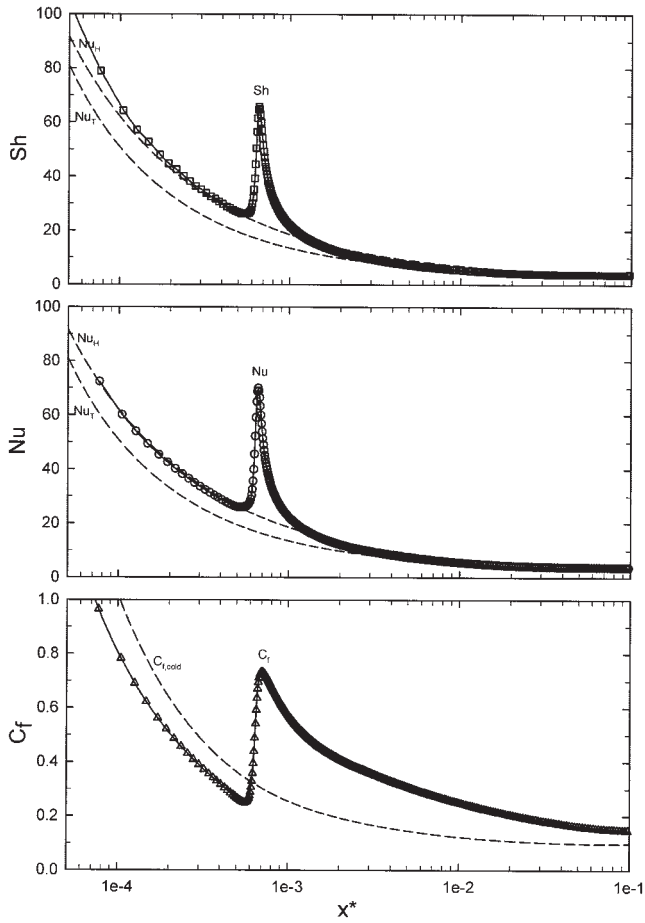

Figure 5. *Sh* number, *Nu* number, and friction coefficient (C_f) under reactive conditions (Table 1) and nonreactive conditions (Nu_T, Nu_H; $C_{f,cold}$) as function of *x.**

Table 2. Kinetic Parameters and Inlet Propane Mass Fraction for the Simulations of Figure 6 and Figure 7

	k_0 (mol/m^2 s)	$\Delta E/\bar{R}$ (K)	$Y_{C3H8,in}$
red_Ea1	3.0	2180	0.09
red_Ea2	87.6	4360	0.03
red_Ea3	$2.28 \cdot 10^2$	5450	0.03
k_0 (base case)	$1 \cdot 10^6$	10869	0.015

Nusselt numbers calculated using the boundary conditions of constant wall temperature and constant wall flux, because neither of these two boundary conditions represents the actual boundary condition.[13] Instead *Nu* exhibits a spike, which is about 3 times the value of *Nu* predicted by the corresponding correlations at the same location. The increase in heat transfer efficiency can be addressed to the effect of ignition of increasing the radial gradients.

Also the friction coefficient C_f exhibits a spike in the light-off region. In Figure 5 C_f is compared to the corresponding $C_{f,cold}$ for the nonreactive case. In the absence of reaction, $C_{f,cold}$ decreases from the inlet value to the corresponding value for developed laminar flow, which can be safely considered corresponding to 64/Re,[27] accompanying with its trend the exhaustion of the entrance effects along the ducts. In the presence of the surface reaction, prior to light-off C_f exhibits a decreasing trend similar to $C_{f,cold}$, but slightly different values due to the occurrence of the superficial reaction that, even though proceeding with a slow rate, affects the fluid-wall interface drag by changing the wall temperature and, hence, the radial velocity gradient. At the ignition C_f suddenly increases from 0.25 up to 0.74, due to the development of new radial profiles of velocity, which resembles for some aspects the entrance effect. Downstream, C_f tends to the asymptotic value for developed laminar flow.

Is ignition a new entrance effect?

The ignition of the superficial reaction induces a perturbation, which is responsible for a significant enhancement of heat, mass, and momentum transfer, in a way that is comparable for some respects to the entrance effects. When the numerical scheme adopted in the solution is not adequate, and when the ignition is conceived by the model as a bifurcation point, with a discontinuous jump from an extinguished solution to an ignited solution, the spike that can be observed in the *Nu* trend can also be addressed to the occurrence of the Gibbs phenomenon.[9]

In this work a control volume approach was instead adopted, with the precise purpose of avoiding the effect of the possible discontinuity due to the passage from the nonignited to the ignited solution. Furthermore, the inclusion in the model of the axial diffusion of momentum, heat, and mass in the gas phase should prevent the ignition from being a discontinuous jump.

Nevertheless, to further evidence the physical meaning of the spike, additional simulations were performed at reduced values of the activation energy of the surface reaction and increased adiabatic temperature rise, as indicated in Table 2. Due to the reduction of the activation energy a very smooth (nondiscontinuous) passage from the extinguished solution to the ignited solution along the monolith is attained. The large and rapid production of heat at the wall, which is reckoned as responsible of the perturbation leading to the spike, is ensured by increasing the ΔT_{ad} with an increase in the inlet fraction of C_3H_8 (Table 2).

In this way the absence of the Gibbs phenomenon is ensured by the smooth ignition, but the large temperature rise persists, causing the variation of density and the perturbation of the fluid flow, even though at slow heat production rate. The activation energy is reduced from the base case (k_0) as much as five times (red_Ea1). Conversely, the propane inlet fraction, and, hence, the adiabatic temperature rise, is increased of a factor 2 (red_Ea2 and red_Ea3) and 6 (red_Ea1).

With respect to the base case, whose results are reported in Figure 1–5, when the activation energy is reduced (red_Ea1, red_Ea2, and red_Ea3) the wall temperature exhibits a smoother increase along the channel length (Figure 6). Nevertheless, a relevant temperature rise is attained within a short distance from the monolith inlet due to the large ΔT_{ad}.

Remarkably, for red_Ea1 the transition of the heat transfer efficiency (*Nu*) from the Nu_H to the Nu_T asymptote, which occurs in the region of the largest temperature increase along the channel, exhibit a slight enhancement that span on the entire length of appreciable difference between wall and bulk temperature. By increasing the activation energy, a more pronounced local enhancement near the light-off arises, for red_Ea2, red_Ea3 up to the formation of a large spike of *Nu* that can be clearly observed in the region of the transition for k_0 (Figure 6).

From the comparison with the corresponding wall and bulk temperature, such enhancement appears to be dependent in intensity and location to the rapid increase of the wall temperature and to the difference between wall and bulk temperatures (Figure 6). In other words, when the reaction rate is faster than heat transfer, and the heat produced is maintained in the proximity of the wall, the perturbation on the heat and momentum boundary layers is stronger, giving rise to a local enhancement of heat transfer.

This concept is illustrated with more clarity in Figure 7, by highlighting the effects of the surface reaction on the flow field, at reducing the activation energy. The radial components of velocity (v) exhibit a second spike along the axial coordinate (Figure 7), in analogy to what observed for *Nu.* The first negative peak is due to the entrance effects, while the second can be ascribed to the effects of the occurrence of the reaction.

For red_Ea1, such effects are spread along the channel, so that the radial velocity is increased globally, but a second peak does not appear. For red_Ea2, red_Ea3, and k_0 a second peak appears, whose intensity increases with the increase of the peak of heat production, also shown in Figure 7.

Indeed, Figure 7 shows that the higher the activation energy, the more concentrated the heat release and the higher its local intensity.

From the results reported in Figure 6 and Figure 7 it can be, hence, concluded that the enhancement of *Nu* in the ignition region has a physical meaning, and depends in intensity and wideness on the rate of heat production at the wall (kinetics and ΔT_{ad}).

Remarkably, the heat transfer efficiency in the cases of red_Ea1, red_Ea2, and red_Ea3 (Figure 6), cannot be strictly assimilated to forced convection with constant wall heat flux (Nu_H) in the region upstream of ignition. In fact, the wall heat flux for reduced activation energy is not constant as for the base

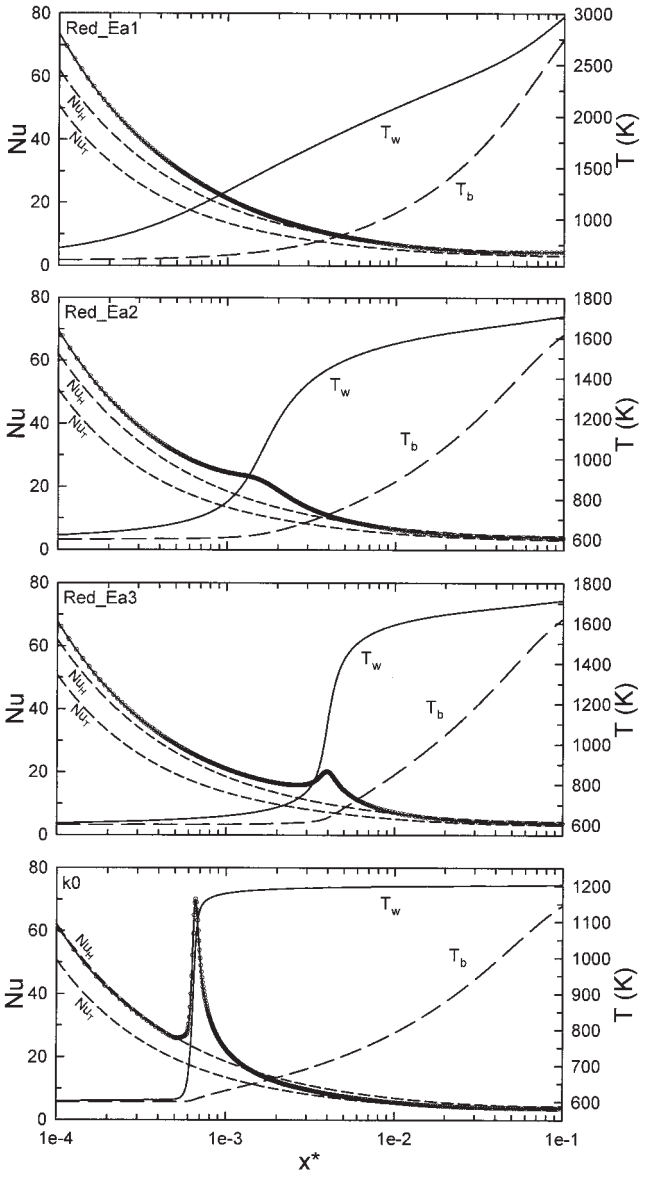

Figure 6. Computed *Nu* number (symbols), Nu_H and Nu_T, and wall (solid lines), and bulk temperature (dashed lines) for red_Ea1, red_Ea2, red_Ea3, and k_0 cases, as referred in Table 2 as function of *x.**

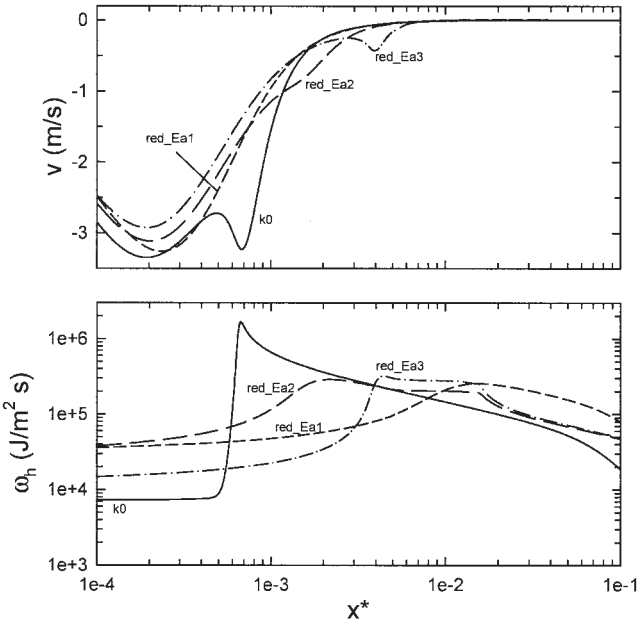

Figure 7. Radial component of velocity at $r = 4.0 \cdot 10^{-4}$ m and wall heat production (ω_h) for red_Ea1, red_Ea2, red_Ea3, and k_0 cases, as referred in Table 2 as a function of *x.**

case (Figure 7), but increases significantly and the local value of *Nu* is higher than Nu_H.

In Figure 6, it is also shown that the *Nu* number shifts along the monolith length together with the ignition location. The ignition position may shift along the reactor channel when the kinetic parameters are changed, and also when the support thermal conductivity changes or during the transient ignition. In all cases what is the relevant result for the wall-bulk phase heat exchange is the link which establishes between the ignition position, the temperature profile and the *Nu* number.

Two-zones model

The perturbation induced by the ignition of the surface reaction on heat, mass, and momentum transfer is analogous for some respects to the entrance effect, and is, thus, herein called "reaction effect."

In the case of a fast exothermic surface reaction, such as for catalytic combustion (characterized by a kinetics more similar to k_0 than to red_Ea1 or red_Ea2), from the standpoint of transfer efficiency, the reactor can be divided into two zones, the first dominated by the entrance effects and the second dominated by the reaction effects, as depicted in Figure 8.

In the first zone, upstream of the ignition location, the interphase heat transfer strictly resembles that occurring in a heat exchanger duct with constant heat flux at the wall. *Nu* is,

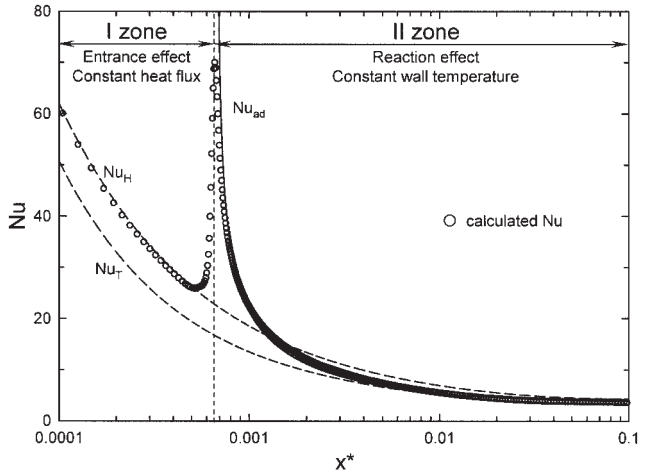

Figure 8. Two-zones model of a catalytic combustor.

In the first zone *Nu* can be compared to Nu_H curve, while in the second zone *Nu* resembles Nu_T, whose origin is shifted to the light-off location (Nu_{ad}).

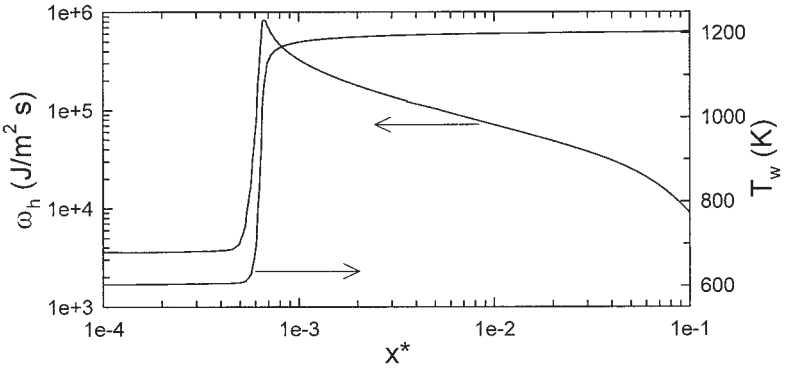

Figure 9. Wall heat flux (ω_h) and wall temperature (T_w) as function of x^* calculated at conditions of Table 1.

hence, superimposed to Nu_H, as shown in the first zone of Figure 8.

In fact, in the first zone the heat flux (ω_h) can be considered with good approximation constant (Figure 9). Analogously, in the second zone the wall temperature (T_w) can be considered with good approximation constant, and far downstream of the ignition, *Nu* tends to the Nu_T asymptotic curve (heat exchange efficiency in ducts with constant wall temperature).

Remarkably, in the passage from the first zone to the second, neither the heat flux nor the wall temperature may be assumed as constant: accordingly *Nu* does not overlap neither Nu_H nor Nu_T. The transition from zone 1 to zone 2 occurs within the region of ignition of the superficial reaction, where a drastic perturbation of the heat, mass, and velocities radial profiles takes place and the wall temperature rapidly increases up to the adiabatic temperature.

The local value of *Nu* moves from the Nu_H asymptotic curve to another transfer efficiency curve, whose peculiarity is that its origin is not anchored to the inlet of the channel (entrance effects), but it is rather anchored to the ignition point, as shown in Figure 8, where such curve is identified by Nu_{ad}.

Theoretically, for a sudden chance of the wall boundary conditions from constant heat flux to constant temperature, Nu_{ad} coincides with the Nu_T curve, whose origin is shifted to the ignition location.

Nevertheless, since in a real case a large number of parameters can influence the rise of the wall temperature from the nonignited to the adiabatic value, such as the activation energy and the pre-exponential factor of the surface reaction,[26] the inlet temperature and the fuel fraction and the wall thermal conductivity,[6] Nu_{ad} deviates from Nu_T in the ignition region, and tends to Nu_T only once the perturbation determined by the reaction ignition has extinguished.

We already showed that by changing the rate of the superficial reaction, by means of the variation of the kinetic parameters, ignition position may vary along the channel, shifting from the inlet towards the outlet at reducing the reaction rate.[26]

When the ignition point is located very close to the channel inlet, and its perturbation is superimposed to the entrance effects, the first zone disappears: *Nu* does not overlap Nu_H, but, starting from a higher value in correspondence of the ignition (and inlet) region, tends to the Nu_T asymptotic curve.

Also the increase of the wall thermal conductivity may have the effect of shifting the ignition point upstream, in the close proximity of the inlet. Young and Finlayson[15] studied the effect of the wall thermal conductivity on the profiles of *Nu* and *Sh* numbers and showed that the effect of axial conduction consists not only in shifting the ignition point towards the inlet, but also in decreasing the magnitude of the efficiency of interphase transfer in the reaction zone. They highlighted that, in the limit of large thermal conductivity, the peak values of *Nu* numbers may disappear, with *Nu* tending to the asymptotic value (even though these conditions are far from the conditions occurring in practice). In addition, according to their results, *Nu* is different from *Sh* in the ignition region, where its peak is lower than *Sh* peak due to the effect of the wall thermal conductivity, since the reaction heat is partitioned between the reaction products leaving the wall and the wall itself.[15]

In a previous article,[6] we have carried out numerical simulations of a monolith channel including the thermal conductivity in the wall (λ_w = 3 W/m K, typical value of a cordierite support), with the difference with respect to the present model that a noncatalytic zone, where the fluid flow was allowed to fully develop, was placed upstream of the catalytic zone, so that the entrance effects were artificially separated from the reaction effects. Numerical results highlighted that in correspondence of the ignition, which under such configuration was anchored to the inlet of the catalytic section, a marked peak of *Nu* occurred.

The introduction of wall thermal conductivity (λ_w = 3 W/m K) in the model used in this article, where the noncatalytic zone of flow development is absent, becomes a useful tool to investigate its effect on the transport efficiency between the surface and bulk gas phase, when superimposed to the entrance effects.

In Figure 10 *Sh* number, *Nu* number, the wall and the bulk temperatures and the radial component of velocity are reported as a function of x^*, computed for the conditions of the base case (Table 1), both in the case of absent thermal wall conductivity (λ_w = 0 W/m K) and for λ_w = 3 W/m K.

When increasing the thermal conductivity of the solid phase, the ignition point shifts upstream and is anchored to the inlet of the channel, as shown by the temperature profiles (Figure 10).

The profiles of the radial component of velocity suggest that in the case λ_w = 0, near the wall ($r = 4.0 \cdot 10^{-4}$ m) two distinct peaks can be clearly detected, being the entrance effect and the reaction effects on fluid dynamics clearly separated. Conversely, for λ_w = 3 W/m K only one peak can be observed, resulting from the overlapping of the entrance and the reaction effects. This peak is more pronounced than for λ_w = 0, being the sum of the perturbations due to the development of the velocity profile and due to the local gas expansion associated to the fast heat release at the ignition. Coherently with the ignition

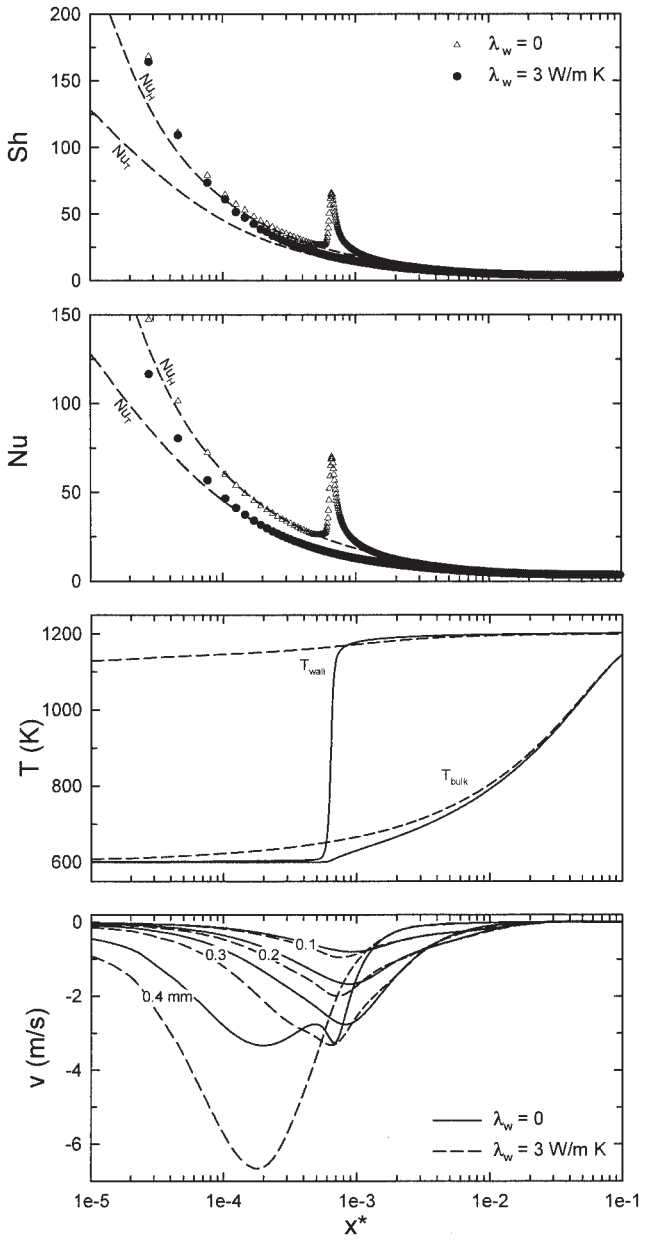

Figure 10. *Nu* and *Sh* numbers, wall and bulk temperature, and radial component of velocity at different values of the radial coordinate plotted as a function of x^*, for $\lambda_w = 3$ W/mK and $\lambda_w = 0$.

location, also the *Nu* peak for $\lambda_w = 3$ W/m K is located at the channel inlet. Hence, the first zone disappears and *Nu* is higher than Nu_T, where the reaction effects are stronger, and then tends to Nu_T (Figure 10).

Nu and *Sh* numbers exhibit some differences in value especially in the ignition region (Figure 10). While for the case $\lambda_w = 0$, the *Nu* spike is slightly higher than the *Sh* spike,[26] the introduction of thermal conductivity in the monolith wall determines a reverse effect on *Nu* and *Sh,* smoothing the *Nu* peak in the ignition region. In agreement with the findings of Young and Finlayson, Figure 10 shows that *Sh* attains a higher value than *Nu.*

From the presented results two main concluding remarks can be derived:

(1) The shift of the *Nu* peak along the geometrical coordinate together with the ignition point is anchored in some way to a reaction coordinate, which can be related to Da_t.

(2) While upstream of ignition *Nu* quite accurately overlaps Nu_H, the *Nu* branch after ignition is dependent on the operating conditions, and on the kinetic and thermal properties of the system.

Nu and Sh correlation

The determination of the *Nu* branch after ignition is, hence, of paramount importance in determining the local value of the interphase transfer along the monolith.

In fact, when ignition is located in the entrance region, *Nu* entirely coincides with such *Nu* branch, as shown for $\lambda_w = 3$ W/m K; conversely, when ignition is located downstream of the entrance region, the value estimated by *Nu* is the result of the interpolation of Nu_H and the *Nu* branch after ignition, as shown for the base case.

In a previous work,[6,26] a new formulation of heat and mass transfer efficiency (Nu_{ad} and Sh_{ad}) was introduced with the aim of capturing the *Nu* trend after the light-off location. Nu_{ad} (Sh_{ad}) exhibit the following features:

(1) it tends to Nu_T far downstream of the ignition point;

(2) it is anchored to the ignition point rather than to the channel entrance;

(3) it embeds the effect of the operating and kinetic parameters.

The definition of Nu_{ad} and Sh_{ad} numbers (Eq. 20 and 21) takes directly into account the effect of the adiabatic temperature rise on transfer efficiency, and is anchored to the ignition location when plotted vs. a dimensionless variable $\Delta\phi_b$ which is equal to the temperature rise $\Delta T_b = (T_{ad} - T_b)/\Delta T_{ad}$ for heat transfer, and $\Delta y_b = (y_{eq} - y_b)/\Delta y_{eq}$ for mass transfer.

$$Nu_{ad} = \frac{-\left.\frac{\partial T}{\partial r}\right|_{r=R} 2R}{(T_{ad} - T_b)} \frac{k_w}{k_b} \tag{20}$$

$$Sh_{ad} = \frac{-\left.\frac{\partial y}{\partial r}\right|_{r=R} 2R}{(y_{eq} - y_b)} \frac{D_w}{D_b} \tag{21}$$

When Nu_{ad} or Sh_{ad} are plotted vs. a modified dimensionless variable $\Delta\phi'_b$ (Eq. 22, where $a = 0.08$, $b = 0.02$), which embeds not only the adiabatic temperature (equilibrium concentration), but also the kinetics of the surface reaction, by means of the Zeldovich number (*Ze,* Eq. 23), and of the inlet Damköhler number (Da_t^{in}, Eq. 24), a good overlap is obtained in a wide spectrum of operating and kinetic parameters

$$\Delta\phi'_b = Ze^a Da_t^{\text{in}^b} \Delta\phi_b \tag{22}$$

$$Ze = \frac{\Delta E}{\bar{R}T_{\text{in}}} \frac{\Delta T_{ad}}{T_{\text{in}}} \tag{23}$$

$$Da_t^{\text{in}} = \frac{L\omega_{C_3H_8}^{\text{in}}}{u_{\text{in}} C_{C_3H_8}^{\text{in}} R} \tag{24}$$

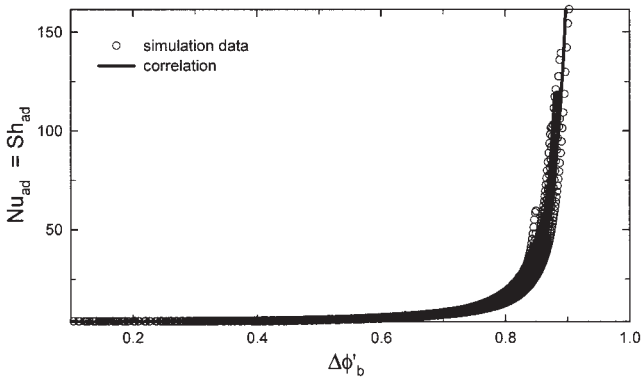

Figure 11. Nu_{ad} (Sh_{ad}) as function of the dimensionless temperature (fuel concentration) gradient for all the simulated cases and its correlation.

At varying the inlet propane concentration (0.015–0.03), the inlet temperature (575–650 K), the pre-exponential factor ($k_0 = 5 \cdot 10^5 - 5 \cdot 10^6$ mol/m^2 s), and the activation energy ($E_a/R_g = 9800$–11300 K^{-1}), the Nu_{ad} and Sh_{ad} curves when plotted vs. ΔT_b, collapse as shown in Figure 11.

The resulting correlation formula for Nu_{ad} is reported in Eq. 25 (regression factor $R^2 = 0.95$). Since Nu_{ad} (Sh_{ad}) is a function only of the bulk temperature, being ΔT_{ad}, Ze, and Da_t^{in} fixed by the inlet conditions and catalyst properties, Nu_{ad} (Sh_{ad}) moves along the monolith with the ignition position, and the same occurs for Sh_{ad}

$$Nu_{ad} = Sh_{ad} = 3.656 + 1.9510^{-4} e^{11.2\Delta\phi_b'/0.9 - 1.03\Delta\phi_b'} \quad (25)$$

It must be highlighted that the slight differences observed between Nu and Sh in the ignition region are smaller than the accuracy of the correlating formula (Eq. 25), and, thus, a unique correlation is indicated for the description of the Nu_{ad} and Sh_{ad} curves.

Moreover, when the wall conductivity plays a significant role, thus introducing a significant difference between Nu and Sh in the ignition region, this correlation does not hold and proper simulations devoted to extend correlation (25) have to be performed.

The correlation of the entire Nu (Sh) curve in the channel can be, hence, achieved by means of the interpolation of the two asymptotic curves upstream of ignition (Nu_H) and downstream of the ignition (Nu_{ad}). Since the ignition position is identified by the local value of the Damköhler number (Da_t), as shown in Figure 1, the interpolation between Nu_H and Nu_{ad} can be attained by the adaptation of the Fetting formula, proposed by Groppi and co-workers for the interpolation of Nu between Nu_H and Nu_T.[10,11]

$$\frac{Nu - Nu_H}{Nu_{ad} - Nu_H} = \frac{Da_t Nu}{(Da_t + Nu)Nu_{ad}} \quad (26)$$

In Figure 12 an example is given of the Nu trend obtained by means of the application of the correlation of Eq. 26, in comparison with numerical simulations for three values of the kinetic parameters. Remarkably, by the use of Nu_{ad} the local Nu enhancement, and the different perturbation effect due to the variation of the kinetics are properly reproduced. The advantage of the correlation (Eq. 26), with the interpolation between Nu_H and Nu_{ad} rather Nu_T, as instead proposed by Groppi et al.,[10,11] is that, especially in the case of fast exothermic surface reactions, as highlighted by the same authors,[10] Nu evaluated as the interpolation of Nu_H and Nu_T may underestimate the actual Nu number in the ignition region.

Figure 13 reports a comparison of the Groppi correlation (dashed line) with the one proposed in this work (solid line) with respect to the computed Nu number (symbols).

The differences between the two correlations, which can be quantified when considering the calculated wall heat flux, based on correlated Nu number, subsists in a relatively small zone (light-off region), comprised between $x^* = 5 \cdot 10^{-4}$ and $5 \cdot 10^{-3}$ (Figure 13), corresponding to 0.002 m of the actual channel. In such zone the adoption of the Groppi correlation leads to the underestimation of the heat fluxes of about 50%. The underestimation of the heat fluxes would lead in a 1-D model to the overestimation of wall temperature and misleading prediction of the light-off location.

In some conditions the ignition point is located very close to the inlet and it superimposes to the entrance region (zone I). This happens for examples at high values of the solid thermal conductivity (Figure 10) and high values of the reaction rate (Figure 6). In these cases the value of the local Damköhler number is very low already at the inlet, and consequently,

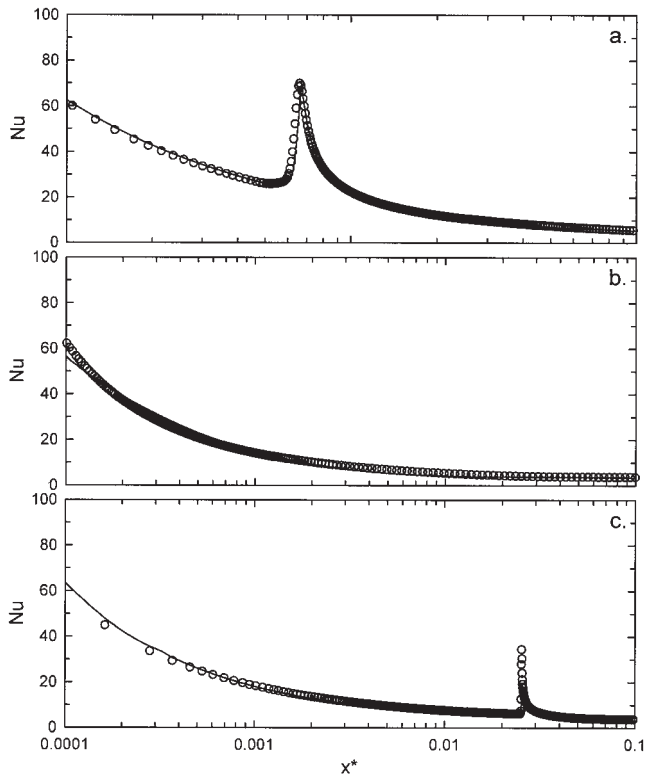

Figure 12. Computed Nu in comparison with correlation of Eq. 7 for: (a) the case of Figure 1 ($k_0 = 10^6$ mol/m^2 s); (b) for an increase of the pre-exponential factor ($k_0 = 5 \cdot 10^6$ mol/m^2 s); (c) for a reduction of the pre-exponential factor ($k_0 = 5 \cdot 10^5$ mol/m^2 s).

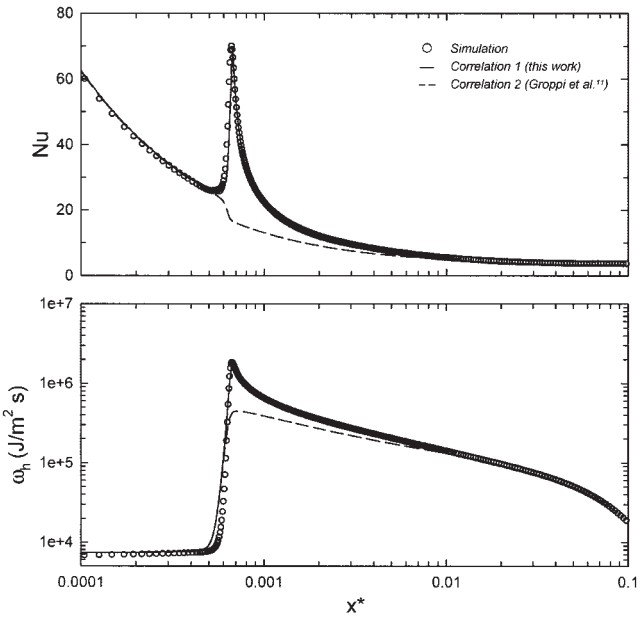

Figure 13. Computed *Nu* number and wall heat flux as a function of the dimensionless axial position in the channel, in comparison with the proposed correlation (Eq. 26), and the literature correlation.[10]

according to correlation (26), *Nu* number coincides with Nu_{ad} along the entire channel length.

Conclusion and Discussion

The numerical simulations of a monolithic reactor presented in this article are aimed at highlighting the role of the coupling of heat, mass, and momentum transfer between the wall and the bulk gas phase in the presence of a superficial reaction.

By means of the analysis of the interaction existing between the position of the ignition and the rate of heat production at the wall on one side and of the interphase heat and mass transfer on the other, the derived results can be divided into two main contributions.

The first one is related to the understanding of the physics underlying the heat and mass transfer between wall and bulk gas phase in the presence of a superficial reaction, while the second one refers to the refinement of an existing *Nu* (*Sh*) correlation able to quantify the heat and mass fluxes along the entire monolith, comprising the ignition region.

First, we showed that the occurrence of light-off, and, hence, the rapid increase of the rate of heat production at the wall, gives rise to a perturbation which can be assimilated to the entrance effect, with the development of radial gradients of temperature, concentration, and velocity, comparable to those occurring at the duct inlet. Consequently, in the region of ignition of the superficial reaction, a local enhancement of the heat and mass transfer between the bulk gas phase and the wall takes place, similar to the enhancement observed at the duct inlet.

It was shown that such *Nu* enhancement is not spurious, that is, due to numerical inaccuracies, such as the Gibbs phenomenon, but has a physical meaning, related not only to the transition of the wall boundary conditions from constant heat flux (upstream of ignition) to constant temperature (downstream of ignition), but also to the perturbation of the flow field. In fact, the local enhancement of the interphase transfer number was observed also under conditions such that the transition of the wall boundary conditions is greatly smoothed, that is, by reducing the activation energy or increasing the thermal conductivity of the solid, when it can only be attributed to the gas expansion associated to the heat production by the surface reaction.

The second contribution consists in the quantification of the *Nu* number under reactive conditions by means of the identification of two zones along the monolith. The first zone located upstream of the ignition position is characterized by a slow rate of reaction, so that the heat and mass fluxes between the wall and the bulk gas phase can be considered constant. In this zone the heat-transfer efficiency may be accurately evaluated by using the correlations for constant wall heat flux in ducts (Nu_H), previously calculated by solving the energy balance equations coupled to the Navier-Stokes equations.

In the second zone, downstream of ignition location, the wall temperature tends to the adiabatic temperature and consequently the heat and mass-transfer efficiency tends to the Nu_T curve, obtained for constant wall temperature ducts. The transition of the transfer efficiency from the first asymptotic curve to the second goes through a local enhancement, which strongly depends on the operating conditions and on the kinetic and thermal properties of the catalytic wall which is not described by the literature available correlation.

It is here proposed to predict the local *Nu* enhancement by means of the modification of an existing interpolation of *Nu* number between Nu_H and Nu_T. *Nu* is now predicted as the interpolation between Nu_H and Nu_{ad} by means of the Fetting formula proposed by Groppi et al.,[10,11] through the value of the local transverse Damköhler number Da_t, which is $\gg 1$ upstream of ignition and $\ll 1$ downstream

$$\frac{Nu - Nu_H}{Nu_{ad} - Nu_H} = \frac{Da_t Nu}{(Da_t + Nu)Nu_{ad}}$$

The asymptotic curve Nu_{ad} (Sh_{ad}), is anchored to the ignition point, tends far downstream of ignition to Nu_T, and is function of the inlet conditions, of the kinetic parameters and of the wall conductivity.

The correlation was developed by investigating a single step reaction, but can be easily extended to detailed surface kinetics. The location of the *Nu* enhancement is anchored to the ignition by means of the value of the local Da_t number, while the Nu_{ad} curve is a function of the *Ze* and Da_t number evaluated at the inlet, and, hence, the determination of *Nu* is only subject to the calculation of *Ze* and Da_t corresponding to the used surface kinetic scheme.

The rate of change of Da_t, and, hence, of transition from a kinetic controlled regime to a mass transfer controlled one, determines, in conjunction with the shape of the Nu_{ad} curve, the width and height of the *Nu* peak. When the ignition is placed at the inlet of the channel, Da_t becomes $\ll 1$ already at the inlet, and *Nu* coincides with Nu_{ad} along the entire monolith.

The great advantage of the present correlation is that, thanks to the anchorage of Nu_{ad} to the ignition location, the local *Nu* enhancement travels with the ignition also during the transient of ignition/extinction of the monolith. As a result, whatever the experimental or theoretical reaction rate and ignition it is

possible to evaluate the heat and mass fluxes coupled to the computation of the temperature profiles and rate of reaction.

Acknowledgments

Almerinda Di Benedetto wishes to warmly thank Prof. Vemuri Balakotaiah for useful and constructive discussions about heat transfer in monolithic reactors.

Notation

C_f = friction coefficient
c_P = specific heat, kJ/kg K
D = diffusion coefficient, m^2/s
Da_t = Transverse Damköhler number
Gz = Graetz number
H, H_i°, h_s = enthalpy, J/kg
$J_{r,i}$, $J_{z,i}$ = radial and axial mass flux of species i, m/s
k_0 = kinetic constant, mol/m^2 s
L = channel length, m
N_s = species number
Nu = Nusselt number
p = pressure, Pa
Pr = Prandtl number
q = heat flux, J/m^2 s
r = radial coordinate, m
R = channel radius, m or universal gas constant
Re = Reynolds number
Sc = Schmidt number
t = time coordinate, s
T = temperature, K
u = longitudinal component of velocity, m/s
v = radial component of velocity, m/s
x^* = dimensionless axial coordinate, $z/(2\,RRePr)$
z = axial coordinate, m
y = mass fraction

Greek letters

ΔE = activation energy, J/mol
λ = thermal conductivity, W/m K
μ = viscosity, Pa s
ρ = density, kg/m^3
τ = stress tensor, kg/m s^2
ω = reaction rate mol/m^2 s, heat of reaction, J/mol s

Subscripts and superscripts

ad = adiabatic
b = bulk
c = convective
C_3H_8 = propane
$cold$ = nonreactive case
eq = equilibrium
h = heat
H = constant heat flux
Hy = hydrodynamic
in = inlet
LO = light-off location
r = radial direction
T = constant temperature
w = wall
y = mass
z = axial direction

Literature Cited

1. Hayes RE, Kolaczkowski ST. *Introduction to Catalytic Combustion.* Amsterdam: Gordon & Breach Science Publishers; 1997.
2. Prasad R, Kennedy LA, Ruckenstein F. Catalytic combustion. *Catalysis Review-Sci Eng.* 1984;26:1–58.
3. Donsì F, Pirone R, Russo G. Oxidative dehydrogenation of ethane over a perovskite-based monolithic reactor. *J of Catalysis.* 2002;209:51–61.
4. Jahn R, Snita D, Kubicek M, Marek M. 2-D modelling of monolith reactors. *Catalysis Today.* 1997;38:39–46.
5. Tischer S, Correa C, Deutschmann O. Transient three-dimensional simulations of a catalytic combustion monolith using detailed models for heterogeneous and homogeneous reactions and transport phenomena. *Catalysis Today.* 2001;69:57–62.
6. Di Benedetto A, Marra FS, Russo G. Heat and mass fluxes in presence of superficial reaction in a not completely developed laminar flow. *Chem. Eng. Sci.* 2003;58:1079–1086.
7. Canu P, Vecchi S. CFD simulation of reactive flows: catalytic combustion in a monolith. *AIChE J.* 2002;48:2921–2935.
8. Donsì F, Caputo T, Di Benedetto A, Pirone R, Russo G. Modeling ethane oxy-dehydrogenation over monolithic combustion catalysts. *AIChE J.* 2004;50:2233–2245.
9. Gupta N, Balakotaiah V. Heat and mass transfer coefficients in catalytic monoliths. *Chem. Eng. Sci.* 2001;56:4771–4786.
10. Groppi G, Tronconi E, Forzatti P. Mathematical models of catalytic combustors. *Catalysis Rev.-Sci. Eng.* 1999;41:227–254.
11. Groppi G, Belloli A, Tronconi E, Forzatti P. A comparison of lumped and distributed models of monolith catalytic combustors. *Chem. Eng. Sci.* 1995;50:2705–2715.
12. Raja LL, Kee RJ, Deutschmann O, Warnatz J, Schmidt LD. A critical evaluation of Navier-Stokes, boundary layer and plug-flow models of the flow and chemistry in a catalytic-combustion monolith. *Catalysis Today.* 2000;59:47–60.
13. Hayes RE, Kolackowski ST. A study of Nusselt and Sherwood numbers in a monolith reactor. *Catalysis Today.* 1999;47:295–303.
14. Heck RH, Wei J, Katzer JR. Mathematical modeling of monolithic catalysts. *AIChE J.* 1976;22(3):477–484.
15. Young LC, Finlayson BA. Mathematical models of the monolith catalytic converter: part II. Application to automobile exhaust. *AIChE J.* 1976;22:343–353.
16. Hayes RE, Kolaczkowski ST. Mass and heat transfer characteristics of catalytic monolith reactors. *Chem. Eng. Sci.* 1994;49:3587–3599.
17. Barresi A, Vanni M, Baldi G. Evaluation of mass transfer coefficients for laminar flow in monolithic reactors with catalytic walls. *Proc. of the CHISA '96 12th Int. Congress of Chem. and Process Eng.* Aug. 25–30, Praha, CZ; 1996.
18. Kee RJ, Rupley FM, Miller JA, Coltrin ME, Grcar JF, Meeks E, Moffat HK, Lutz AE, Dixon-Lewis G, Smooke MD, Warnatz J, Evans GH, Larson RS, Mitchell RE, Petzold LR, Reynolds WC, Caracotsios M, Stewart WE, Glarborg P, Wang C, Adigun O, Houf WG, Chou CP, Miller SF, Ho P, Young DJ. CHEMKIN Release 4.0, Reaction Design, Inc., San Diego, CA; 2004.
19. GRI-Mech Version 3.0 (1999). CHEMKIN-II format; www.gri.org.
20. Toro EF. *Riemann Solvers and Numerical Methods for Fluid Dynamics.* 2nd ed. Berlin: Springer; 1999.
21. Gaskell PH, Lau KC. Curvature-compensated convective transport: SMART, a new boundedness-preserving transport algorithm. *Int. J. of Numerical Methods in Fluids.* 1988;8:617–641.
22. CFD-RC, CFD-ACE+ User Manual, http://www.cfdrc.com, Huntsville, AL, 2002.
23. Van Doormaal JP, Raithby GD. Enhancements of the SIMPLE Method for Predicting Incompressible Fluid Flows. *Numerical Heat Transfer.* 1984;7:147–163.
24. Shah RK, London AL. Laminar flow forced convection in ducts. New York: Academic Press; 1978.
25. Donsì F, Di Benedetto A, Marra FS, Russo G. CFD simulation of heat transfer in a circular channel: effect of the Pe number. *Int. J. of Chem. Reactor Eng.* 2005;3:A36 http://www.bepress.com/ijcre/vol3/A36.
26. Di Benedetto A, Donsì F, Marra FS, Russo G. Heat and mass fluxes in presence of fast exothermic superficial reaction. *Combustion Theory and Modelling,* 2005;9(3):463–477.
27. White FM. Viscous fluid flow. Washington DC: Mc Graw Hill; 2001.

Manuscript received Mar. 4, 2005, and revision received Aug. 3, 2005.